Plasma Science and Technology

PAPER

The enhanced aerosol deposition by bipolar corona discharge arrays

To cite this article: Jiacheng LI *et al* 2021 *Plasma Sci. Technol.* **23** 064010

Plasma Sci. Technol. **23** (2021) 064010 (6pp) https://doi.org/10.1088/2058-6272/abf6ad

The enhanced aerosol deposition by bipolar corona discharge arrays

Jiacheng LI (李嘉诚)[1], **Zhongzheng HUANG** (黄钟政)[1], **Dawei LIU** (刘大伟)[1,*] **and Kuanlei ZHENG** (郑宽磊)[2,*]

[1] State Key Lab of Advanced Electromagnetic Engineering and Technology, School of Electrical and Electronic Engineering, Huazhong University of Science and Technology, Wuhan 430074, People's Republic of China
[2] School of Electrical and Information Engineering, Wuhan Institute of Technology, Wuhan 430205, People's Republic of China

E-mail: liudw@hust.edu.cn and kuanlei_zheng@wit.edu.cn

Received 15 December 2020, revised 7 April 2021
Accepted for publication 9 April 2021
Published 29 April 2021

Abstract

The corona discharges provide an efficient way to induce precipitation or eliminate fog by increasing ion density in the open air. In this paper, one bipolar corona discharge array (positive and negative high voltage coupled simultaneously) which can generate high densities of positive and negative ions is developed. The comparison between bipolar corona discharge array and unipolar corona discharge array (positive or negative coupled only) indicates that bipolar corona discharge array can generate ~3 times higher ion density than unipolar corona discharge array. More charged aerosols are produced through collisions between ions and aerosols. The collision rate between aerosols is increased substantially by the attractive forces between positively and negatively charged aerosols. The deposition of aerosols induced by bipolar discharges is 25.7% higher than that of unipolar discharges at the humidity super-saturation condition. Therefore, the bipolar corona discharge system is a new option for the large scale ion sources used for artificial weather modification.

Keywords: corona discharges, charged aerosols, bipolar discharges

(Some figures may appear in colour only in the online journal)

1. Introduction

In recent years, as the intensification of global warming, extreme weather events such as droughts and floods have become more frequent [1–4]. The lack of water in Africa and Asia have affected local agriculture, industries and even human health [4]. Forest fires happened more and more frequently in China, Australia and America [5, 6]. Artificial rainfall provides an effective way to alleviate the drought problem, which is commonly realized by dispersing man-made condensation nuclei (table salts, dry ice, silver iodide, etc) to alter physical chemical processes within the cloud [7–10].

Different from the above hygroscopic particles, the charged aerosols produced through the collisions between ions and aerosols can act as condensation nuclei under super-saturation conditions. Changes in cloudiness of the Earth are directly affected by ions generated by galactic cosmic rays in atmosphere directly [11–14]. Recently, plasma or laser-based technologies were used to generate charged condensation nuclei to try to realize fog elimination or rain enhancement [15–17].

For example, a rainfall enhancement trial using a ground-based ionization technology was conducted in the Hajar Mountains in western Oman over a period of 170 d (May to October) in 2013. A positive and significant rainfall enhancement effect attributable to the operation of the emitters was observed [18]. The large corona discharge system with the 7.2 km long wire electrode and applied voltage of −90 kV was installed. This system generated a large-scale (30 m × 23 m × 90 m) high ion density coverage [19]. The following cloud chamber experiments (with relative humidity of (130 ± 10)%) indicate that charged aerosols produced by

* Authors to whom any correspondence should be addressed.

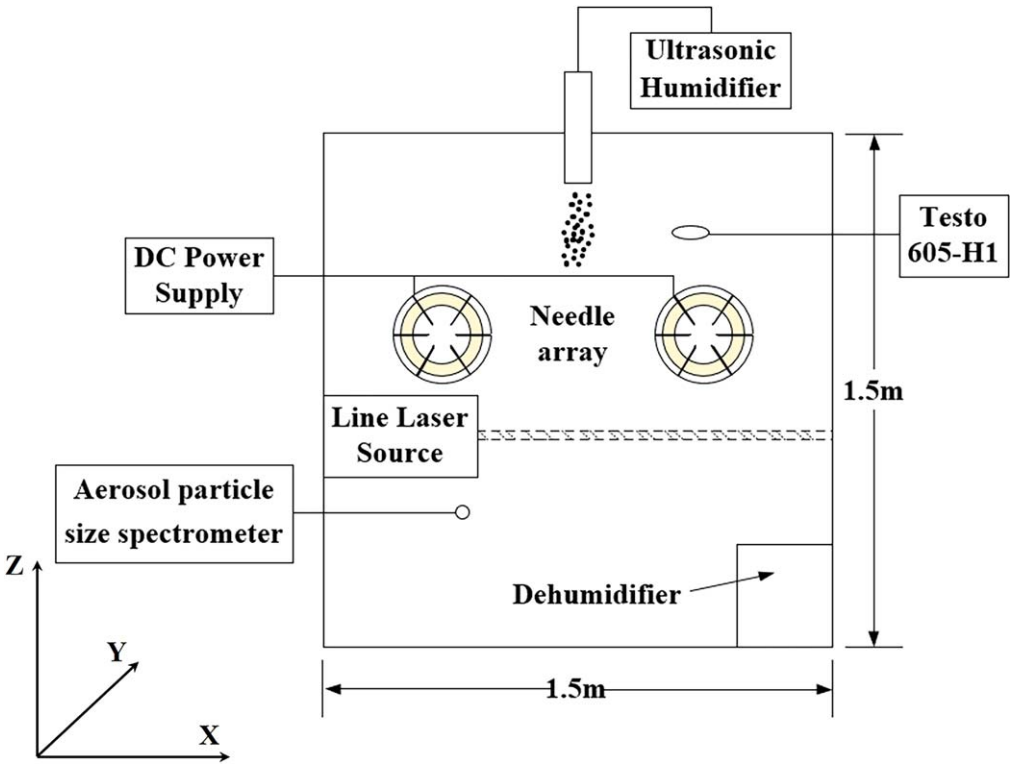

Figure 1. The cloud chamber (6.75 m^3) used to study the ion distribution (side view) and enhanced condensation by corona discharge array. The distance between two needles array electrodes is 0.5 m.

ions of the corresponding density enhanced the deposition of aerosol by 38% [19].

These corona discharge systems are usually driven by negative high voltage DC power supply, because the negative corona discharge systems have the advantage of lower corona onset voltage and higher ion density generation [20]. However, the collision between the negative charged condensation nuclei and neutral aerosols is still limited compared with the collision between negative and positive charged aerosols [21, 22]. Therefore, the combination of negative and positive corona discharge systems (bipolar corona discharges) has the potential to increase the deposition efficiency of aerosols.

In this paper, the discharge characteristics of bipolar discharge array such as current and voltage characteristics, the discharge structure and optical emission spectroscopy (OES) are studied. The ion densities of bipolar discharges and unipolar discharges are measured to estimate the effect of charge on the deposition of aerosols. The calculation on the collision rate between aerosols suggests that the collision rate between negative and positive charged aerosols is higher. The further experiment study on the growth dynamics and deposition efficiency of charged aerosols at humidity super-saturation conditions confirms the advantages of bipolar discharges.

2. Experiment setup and numerical model

The experiment is conducted in the cloud chamber with the size of 1.5 m × 1.5 m × 3 m (figure 1). The humidity is controlled at (130 ± 10)% by the ultrasonic humidifier (Midea SC4E40) and the air drier (Gree DH40EF). The deionized water and 3 layers of grounded mesh electrodes connected to the output of the humidifier are used to neutralize charged aerosols in the cloud chamber. The air temperature inside the cloud chamber is (2 ± 1) °C. The linear laser source (Huisite303D) is used to light up the specific position within the chamber. The line laser source includes the 650 nm 200 mW red high power line laser module. The line width of laser beam is about 0.5 mm. The digital camera (Nikon D800) with a microscopic lens is used to take the picture of the liquid aerosols. The microscope–camera set-up enabled variable magnification between a 1.0 mm × 1.5 mm (for condensation of aerosols) and a 10.0 mm × 15.0 mm (for corona discharges) fields of view. The exposure time of aerosols image and discharge image is 0.05 s and 1 s, respectively. The aerosol spectrometer (GRIMM 1.109) is used to measure the aerosol density (aerosol diameter in the range of 0.25–32 μm) at the condition of humidity <95%. The deposition of aerosol is measured by a collector (a plate with diameter of 40 cm) placed at the bottom of the cloud chamber.

Two corona discharge arrays with the distance of 0.5 m are used to increase the ion density inside the cloud chamber. Each corona discharge array consists of 6 stainless steel needle electrodes with the diameter of 0.25 mm. These needles are placed with 60° intervals. The tip of needles (30 μm in diameter) points to the center of the circle (figure 1). The applied voltages on two discharge arrays are +20 kV (positive corona discharges), −20 kV (negative corona discharges), and +/−20 kV simultaneously (bipolar discharges) (High voltage DC power supply:

Technix 44-2015). An optical spectrometer (Ocean optics USB4000+) is used to measure the OES of the corona discharge. The ion density inside the chamber is measured by the ion counter (Air Ion Counter), whose measurement range is 10 ions cm^{-3}–2×10^8 ions cm^{-3}. It can work properly in the temperature range of −10 °C to 50 °C, and wind speeds <15 km h^{-1}. The OES and ion density measurements are carried out at the ordinary humidity (75% RH or less), because these devices cannot work at the high humidity conditions.

The collision rate between the neutral and charged aerosols is calculated to study the effect of charges on the aerosols. The collision rate R_T considers effects of the electrical, phoretic and diffusive forces, which include a solution to the diffusion-convection equation, provided the electrical force, as for thermophoretic and diffusophoretic forces, varies inversely with the square of the distance from the center of aerosols [10]. The collision rate is calculated by

$$R_T = \frac{4\pi B_p C}{\exp(B_p C/D_p f_p A) - 1}, \tag{1}$$

where D_p is diffusion coefficient of particles, B_p is their mobility, f_p is a ventilation coefficient to account for the increase in diffusive flux due to the liquid aerosol moving through the air, and C is the sum of constants for the non-diffusive forces, for example, $C = C_e + C_{Th} + C_{Df}$, where the constants on the right hand side are proportional to the inverse square electrical, thermophoretic and diffusophoretic forces respectively [22, 23].

$$C_{Th} = -\frac{12\pi\eta_a r(k_a + 2.5k_P N_{Kn})k_a a(T_\infty - T_a)\bar{f}_h}{5(1 + 3N_{Kn})(k_P + 2k_a + 5k_P N_{Kn})p}, \tag{2}$$

$$C_{Df} = -6\pi\eta_a r\frac{0.74D_a M_a(\rho_{v,\infty} - \rho_{a,\infty})\bar{f}_v}{(1 + aN_{Kn})M_\varpi \rho_a}, \tag{3}$$

where k_a is the thermal conductivities of air, and k_P is the thermal conductivities of aerosol particle material, η_a is air's dynamic viscosity, D_v is the diffusivity of water vapor in air, T is air temperature, r is the diameter of aerosol, the Knudson number $N_{Kn} = \lambda_a/r$, with λ_a the mean free path length of air molecules, p is the air pressure, ρ_v is the density of water vapor in air, M_a is the molecular weight of air, M_ω is the molecular weights of water, ρ_α is the density of air and $\alpha = 1.26 + 0.40\exp(-1.1\ N_{Kn}^{-1})$.

The electric force between one charged and the other uncharged aerosols, C_e, considers the image charge [24] induced on the object by charges on the charged aerosol, there is a short range attractive force proportional to q^2, in addition to the long-range force. This is the IC expression

$$C_e = \frac{1}{4\pi\varepsilon_0}\left[Qq - \frac{q^2 A}{a}\left\{\frac{1}{(1 - A^2/b^2)^2} - 1\right\}\right], \tag{4}$$

where, Q is the charges of larger spherical objects, A is the diameter of larger spherical objects, q is the charge of smaller object, a is the diameter of smaller objects, b is the gap between the center of liquid aerosols, ε_0 is the vacuum permittivity.

The electric force between two charged aerosol with charges of opposite polarity is

$$C_e' = \frac{Q_1 Q_2}{4\pi\varepsilon_0 b^2}, \tag{5}$$

where Q_1 and Q_2 are charges of two spherical objects, and b is the gap between the centers of them.

3. Results and discussion

3.1. The discharge characteristics of bipolar corona discharges array

The photos of bipolar corona discharges (+/−20 kV) arrays are shown in figure 2. Because of the low brightness of corona discharges, the exposure time of all photo is set at 1 s. The zoomed in sub-figure (top right corner) of figure 2(a) shows that the positive corona discharge on a single pin electrode has a homogenous glow and no filamentary discharge structure. The similar structure is also observed for the positive corona discharge at medium pressure (1–100 Torr) [25, 26]. The current of positive corona discharge array is (540 ± 15) μA. The negative corona discharges shown in the zoomed picture (top left corner) of figure 2(b) consist of bright spot near the pin electrode and the outer filaments discharges [25, 26]. The current of negative corona discharge array is (624 ± 45) μA. Although the discharges photos of two discharge arrays positive or negative coupled only are not shown, the discharge currents of positive and negative corona discharges are (750 ± 55) μA and (920 ± 50) μA, respectively. They are less than the sum of positive and negative discharge current of bipolar discharges.

Figures 2(b) and (c) indicate that excited N_2 or N_2^+ species dominated OES of positive and negative corona discharges. The peaks in figures 2(b) and (c) correspond to the OES of nitrogen 2nd positive electronic transition $N_2((\nu' = 1) \rightarrow (\nu'' = 4))$ at 399.7 nm, $N_2((\nu' = 0) \rightarrow (\nu'' = 2))$ at 380.4 nm, $N_2((\nu' = 0) \rightarrow (\nu'' = 1))$ at 357.6 nm, $N_2((\nu' = 0) \rightarrow (\nu'' = 0))$ at 337 nm, $N_2((\nu' = 1) \rightarrow (\nu'' = 0))$ at 315.8 nm. The comparison of OES between positive and negative corona discharges suggests that the ratio of 391.4 nm ($N_2^+(B^2\sum_u^+ - X^2\sum_g^+(0 - 0))$) intensity over peak at 337 nm of positive discharges is smaller than that of negative discharges. Energetic electrons are needed to generate $N_2^+(B^2\sum_u^+)$ in excited state of 391.4 nm optical emission [20]. More energetic electrons produced by the strong electric field in the sheath near the negative coupled needle electrode are the key reason for the generation of $N_2^+(B^2\sum_u^+)$ in the excited states and the corresponding higher ratio of 391 nm/337 nm of negative corona discharge [27, 28]. The mass spectrometry measurement of air corona discharges indicates that most of positive ions generated by discharges eventually transform into the ion clusters of $H_3O^+(H_2O)_n$ [29] and most of negative ions eventually transform into the ion clusters of $NO_3^-(H_2O)_n$ [30].

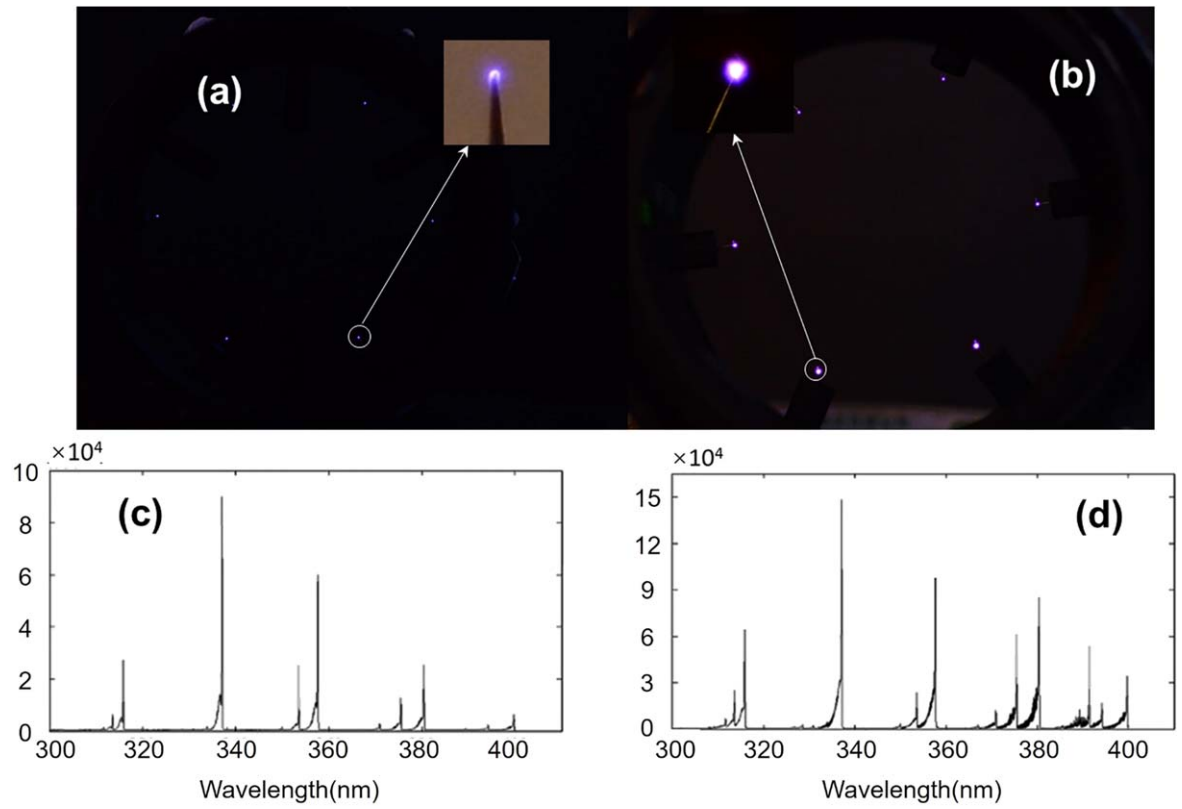

Figure 2. Images and OES of +/−20 kV corona discharge array. (a) Image and (c) OES of positive corona discharge arrays. (b) Image and (d) OES of negative corona discharge. The inserted pictures of (a) and (b) are zoomed in picture of discharges on the needle electrode.

3.2. Ions generated by corona discharges array

Figure 2 shows that the corona discharges only occupy a small volume near the tip of needle electrodes. The boundary of discharge region is usually thought as the position where the electric field is 80 Td (reduced electric field 1 mm range from the electrode) [31]. The ion density inside the discharge region is 10^{11}–10^{13} cm^{-3}. Because of the migration along the electric field and diffusion, the ion density decreases as the distance from the pin electrode increases. The ion density decreases to 10^{8} cm^{-3} with the reduced electric field ~20 Td at the boundary of the discharge region, usually 0.5 cm from the electrode [31–34].

Figure 3 shows that the negative ion density of negative corona discharge decreases from 13.1 × 10^{6} cm^{-3} to 2.5 × 10^{6} cm^{-3} as the distance from the pin electrode increases from 25 to 70 cm. The negative ion density generated by negative corona discharges is about 21% higher than positive ion density generated by positive corona discharges within the range of 40 cm from electrode, afterwards, their densities are roughly same. The sum of ion densities of bipolar discharges is higher than the negative ion density of negative corona discharges within 40 cm from the electrode. The sum of negative ion density and positive ion density of bipolar discharges is about 3 and 2.5 times as high as positive ions of positive corona discharge, and negative ion density of negative corona discharge, respectively. The mutually-reinforcing electric field of bipolar corona discharge results in the higher ion density [35].

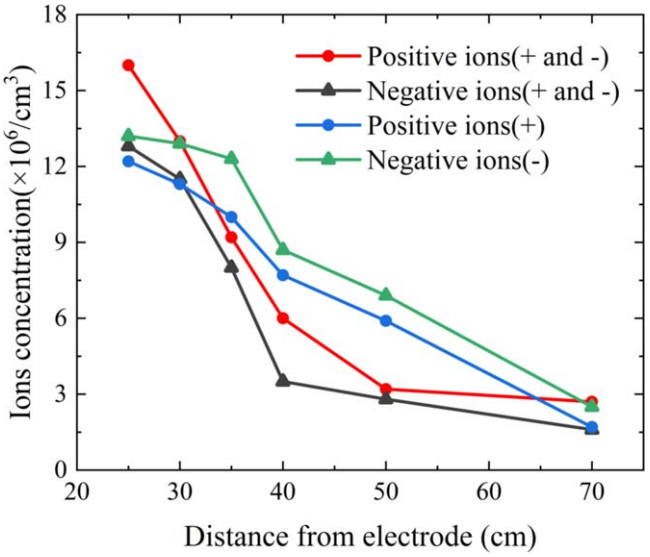

Figure 3. The distributions of ions generated by bipolar corona discharges and single corona discharge.

3.3. The enhanced precipitation by charged nucleus

The total density of aerosol with the diameter of 0.25–10 μm is 1.8 × 10^{9} m^{-3} at the humidity of 70%, and it increases to 2.9 × 10^{10} m^{-3} at the humidity of 95%. Although the aerosol particle size spectrometer can not work properly at the condition of humidity supersaturation (relative humidity (130 ± 10)%), the increase of total density of aerosol is expected to be not more

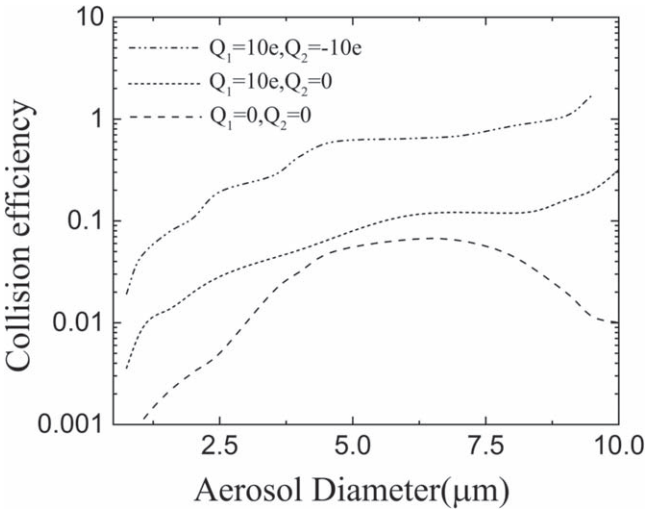

Figure 4. The collision efficiency between a charged 5 μm diameter aerosol and aerosols with diameter of 1 to 10 μm. Q_1 is the charge of 5 μm diameter aerosol. Q_2 is the charge of aerosols with diameter of 1 to 10 μm.

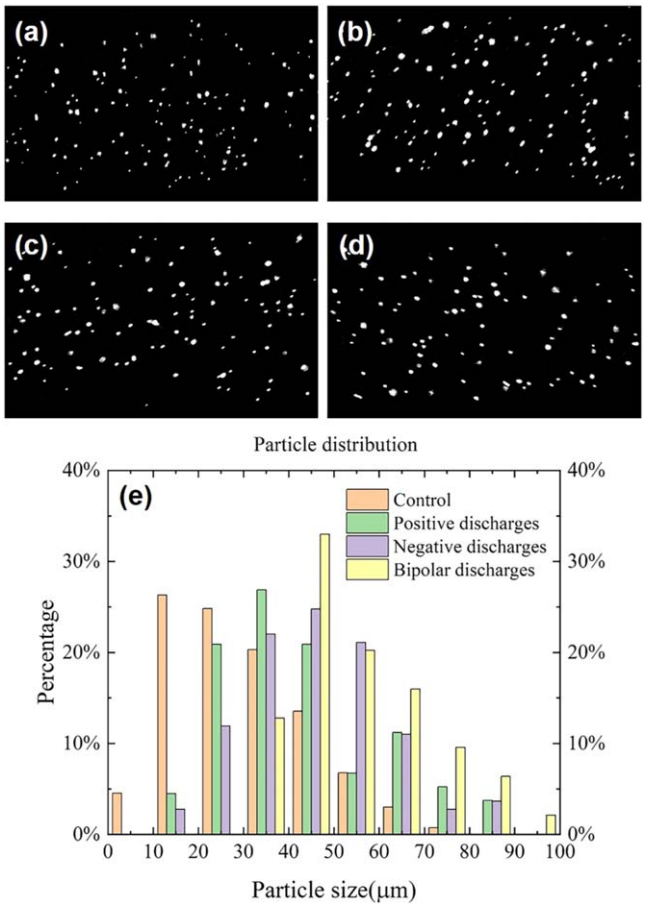

Figure 5. Photos of aerosols in the laser path for (a) control group, (b) positive corona discharge, (c) negative corona discharges, (d) bipolar discharges. Photos are taken at 5 min after the experiment start. (e) The distribution of aerosols size for the control group, positive corona discharge, negative corona discharges, and bipolar discharges (calculated according to (a), (b), (c) and (d)).

than an order of magnitude [36]. The ion density (1.5×10^7–1.1×10^6 cm^{-3}) at 25 –70 cm from the electrode is much higher than the aerosol density, which means the aerosols have ample opportunities to be charged [15, 19, 37].

The aerosols with diameter >0.7 μm are mainly charged through the drift of ions on the field lines intersecting aerosols' surfaces (field charging), as they move across the corona discharges volume or the region close to the electrode. As aerosols move to the region a bit far from the corona discharges, the diffusion of ions to aerosols' surfaces facilitates charging of aerosols (diffusion charging) [38].

Lots of aerosols are charged by the field charging and diffusion charging mechanism. Different from the neutral aerosols which only can collide with each other through thermophoretic and diffusophoretic forces, the electric force of charged aerosol facilitates the collision between aerosols [39–41]. The unipolar charged aerosols (positive or negative charges only) can induce the image charges in adjacent aerosols, and the consequent electric forces are the short range attractive forces and long range repulsive forces. Figure 4 shows the collision rate between charged aerosol (5 μm (in diameter) and 10e (charge number)) and neutral aerosols (1–10 μm) is about 1.5–10 times as high as the collision rate between 5 μm uncharged aerosols and neutral aerosols (1–10 μm).

The bipolar corona discharges generate high density of positive and negative ions (figure 3), simultaneously, the collision between these ions and aerosols generates lots of positively and negatively charged aerosols. The electric force between positively and negatively charged aerosols is attractive force only [21]. Therefore, the collision rate between positively charged aerosol (5 μm and 10e (charge number)) and negatively charged aerosols (1–10 μm, −10e (charge number)) is about 10 times as high as the collision rate between unipolar charged aerosols and neutral aerosols (figure 4) [22].

The size distributions of liquid aerosols generated by natural deposition case (control group) and discharges group (positive, negative and bipolar discharges) inside the chamber are compared in figure 5. The liquid aerosols mainly distributed in 10–30 μm range for the natural deposition. Larger liquid aerosols are generated through the increased collisions between charged aerosols and uncharged aerosols, therefore, the liquid aerosols diameter distributed mainly in 20–60 μm range for positive and negative discharges, and the liquid aerosols of negative discharges are bigger because of higher ion density than positive corona discharges. Because of the even higher ion densities of bipolar discharges and higher collision rate between bipolar charged aerosols, the liquid aerosols distributed mainly in 40–70 μm for bipolar discharges.

The deposition amounts of aerosols are compared in figure 6. The deposition amounts of control group, positive corona discharge, negative corona discharge, and bipolar discharges are 69.9 mg, 88.6 mg, 106.2 mg, and 133.5 mg, respectively. The deposition amount of charged aerosols generated by bipolar discharges is 25.7% more than that of negative discharges, which is consistent with larger aerosol particle generation of bipolar discharges shown in figure 5. The comparison of deposition efficiency of charged aerosols proves greater application potential of bipolar discharges.

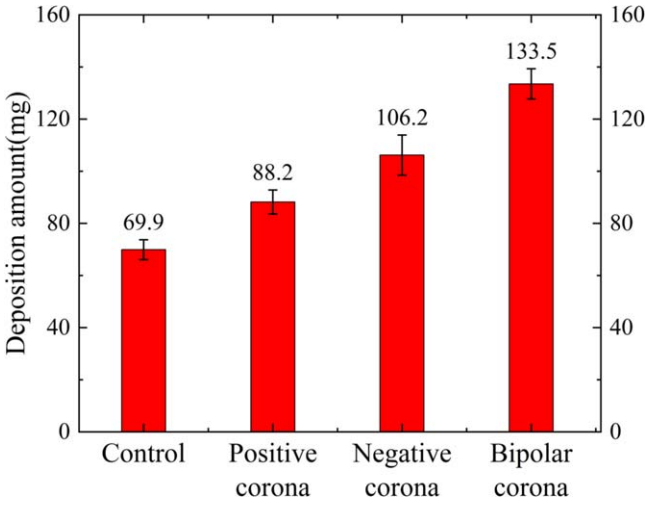

Figure 6. The deposition of aerosols of control, positive corona discharges, negative corona discharges, and bipolar discharges on the collector at the time of 10 min after the experiment started.

4. Conclusion

The bipolar corona discharge array is used to generate the charged aerosols in the cloud chamber. Compared with unipolar corona discharge array, the bipolar corona discharges array can produce ∼3 times higher ion density, and the consequent higher collision efficiency between positive and negative charged aerosols, eventually enhance precipitation by 25.7% under humidity super-saturation conditions. The bipolar corona discharges provide a new technical option for the implementation of artificial rainfall.

Acknowledgments

This study is supported by National Key Research and Development Plan of China (No. 2016YFC0401001).

References

[1] Coumou D and Rahmstorf S 2012 *Nat. Clim. Change* **2** 491
[2] Wallace J M *et al* 2014 *Science* **343** 729
[3] Schiermeier Q 2018 *Nature* **560** 20
[4] Chen H P, Sun J Q and Chen X L 2013 *Atmos. Oceans Sci. Lett.* **6** 8
[5] Stocks B J *et al* 1998 *Clim. Change* **38** 1
[6] Drossel B and Schwabl F 1992 *Phys. Rev. Lett.* **69** 1629
[7] Yang Y *et al* 2018 *IEEE Trans. Plasma Sci.* **46** 1786
[8] Zhang J, Jiao J J and Yang J 2000 *Eng. Geol.* **57** 31
[9] Hudson J G 1993 *J. Appl. Meteor.* **32** 596
[10] Hindman E E II, Hobbs P V and Radke L F 1977 *J. Appl. Meteor. Climatol.* **16** 745
[11] Pierce J R and Adams P J 2009 *Geophys. Res. Lett.* **36** L09820
[12] Carslaw K S, Harrison R G and Kirkby J 2002 *Science* **298** 1732
[13] Harrison R G 2000 *Space Sci. Rev.* **94** 381
[14] Svensmark H *et al* 2017 *Nat. Commun.* **8** 2199
[15] Tan X *et al* 2016 *IEEE Trans. Plasma Sci.* **44** 2724
[16] Khain A *et al* 2004 *J. Appl. Meteor. Climatol.* **43** 1513
[17] Henin S *et al* 2009 *Appl. Phys. Lett.* **95** 091107
[18] Chambers R *et al* 2016 *Arab. J. Geosci.* **9** 491
[19] Ma S X *et al* 2020 *Atmos. Chem. Phys.* **20** 11717
[20] Raizer Y P 2001 *Gas Discharge Physics* ed V I Kisin trans (Berlin: Springer)
[21] Khain A *et al* 2005 *Q.J.R. Meteorol. Soc.* **131** 2639
[22] Wang P K, Grover S N and Pruppacher H R 1978 *J. Atmos. Sci.* **35** 1735
[23] Zhou L M, Tinsley B A and Plemmons A 2009 *J. Geophys. Res. Atmos.* **114** D18201
[24] Tinsley B A *et al* 2000 *J. Atmos. Sci.* **57** 2118
[25] Antao D S *et al* 2009 *Plasma Sources Sci. Technol.* **18** 035016
[26] Ercilbengoa A E, Spyrou N and Loiseau J F 2001 *J. Phys. D: Appl. Phys.* **34** 584
[27] Liu D W, Iza F and Kong M G 2009 *Appl. Phys. Lett.* **95** 031501
[28] Liu D W, Iza F and Kong M G 2009 *Plasma Process Polym.* **6** 446
[29] Ito T *et al* 2015 *Plasma Med.* **5** 283
[30] Sekimoto K and Takayama M 2007 *Int. J. Mass Spectrom.* **261** 38
[31] Chen J H and Davidson J H 2003 *Plasma Chem. Plasma Process.* **23** 83
[32] Riba J R, Morosini A and Capelli F 2018 *Energies* **11** 2671
[33] Yao X M *et al* 2019 *Chem. Eng. J.* **362** 339
[34] Zhang B, He J L and Ji Y M 2019 *IEEE Trans. Dielectr. Electr. Insul.* **26** 1403
[35] Zhang L *et al* 2014 *J. Appl. Phys.* **116** 113301
[36] Hinds W C 1999 *Aerosol Technology: Properties, Behavior, and Measurement of Airborne Particles* (New York: Wiley)
[37] Zhang Y Z *et al* 2020 *High Volt.* (https://doi.org/10.1049/hve2.12036)
[38] Jidenko N and Borra J P 2012 *J. Hazard. Mater.* **235–236** 237
[39] Tinsley B A *et al* 2008 *Rep. Prog. Phys.* **71** 066801
[40] Wang P K *et al* 2003 *J. Geophys. Res.* **108** 4194
[41] Zhou L M *et al* 1998 *Energy Fuels.* **12** 1191